ANZIAM J. (First published online 2024), page 1 of 27*
doi:10.1017/S1446181124000257
*Provisional—final page numbers to be inserted when paper edition is published

DISSIPATION OF WAVE ENERGY AND MITIGATION OF WAVE FORCE BY MULTIPLE FLEXIBLE POROUS PLATES

ANJAN SASMAL[1] and SOUMEN DE[1]✉

(Received 28 July, 2024; accepted 22 October, 2024)

Abstract

The hydroelastic interaction between water waves and multiple submerged porous elastic plates of arbitrary lengths in deep water is examined using the Galerkin approximation technique. We observe the influence of flexible porous plates of arbitrary lengths by analysing the reflection coefficient, dissipated energy and wave forces acting on the plates. Results are presented for various values of angle of incidence, separation lengths of plates, porosity levels, submergence depth and flexural rigidity. The convergence and accuracy of the method are verified by comparing the results with existing literature. The significant impact of flexural rigidity in the presence of porosity on wave reflection, dissipated energy and wave forces is demonstrated. Moreover, a notable reduction in wave load is observed with an increase in the number of plates.

2020 *Mathematics subject classification*: 76B.

Keywords and phrases: water wave interaction, reflection and transmission coefficients, flexible porous plates, wave force, energy dissipation, Galerkin approximation.

1. Introduction

The interaction of surface gravity waves with submerged breakwaters has been a subject of significant research and interest among ocean engineers and coastal scientists. Submerged breakwaters, designed to mitigate the impact of waves on coastal regions, play a crucial role in wave energy dissipation and sediment redistribution. Their effectiveness hinges on several factors including their geometrical configuration, structural integrity, material composition and placement relative to the shoreline. Traditional rigid breakwaters often fail under substantial wave loads, leading to collapse and ineffective protection. To address these challenges, hydroelastic analysis has gained considerable attention due to its critical role in the design of various engineering structures across multiple fields, including coastal, marine, offshore, aerospace

[1]Department of Applied Mathematics, University of Calcutta, 92, A.P.C. Road, Kolkata 700 009, India; e-mail: anjaniitg@gmail.com, soumenisi@gmail.com

and civil engineering. The study of the interaction between fluid and structures, in such a way that the hydrodynamic force of the fluid and the elastic force of the solid body are considered, is referred to as hydroelasticity of marine structures [13, 47]. In recent years, there has been significant growth in the study of hydrodynamic performance of flexible/elastic porous structures. The flexible structures provide an additional feature of wave attenuation through structural deformation compared with a rigid structure. Further, flexible structures are light in weight, cost-effective, reusable and environmentally friendly compared with their rigid counterparts.

Over the past few decades, there has been substantial research interest in the problem of water wave scattering by fixed, rigid obstacles of various geometrical shapes. Dean [9] was among the first to tackle the issue, solving the problem of time-harmonic waves normally incident on a vertical barrier extending downward from a point below the free surface using complex variable methods. Shortly after, Ursell [45] derived the solution for the complementary problem of a vertical barrier extending upwards through the free surface from a point below the free surface. Subsequently, several researchers developed more complex explicit solutions for vertical barrier problems in both infinitely deep and finite-depth water. These researchers included Porter [31], Smith [41], Williams [46], Losada et al. [22], Porter and Evans [32], Chakrabarti et al. [4] and others who focused on single barrier scattering problems. Significant progress in the study of wave interaction with two, three or more thin identical or nonidentical vertical barriers was made by Levine and Rodemich [19], Jarvis [16], Evans and Morris [10], Newman [29], Morris [28], McIver [26], Isaacson et al. [14], De et al. [8], Roy et al. [33] and others.

The interaction of water waves with vertical elastic bodies has not been extensively studied within the framework of linear theory, resulting in limited mathematical techniques available in the literature. Meylan [27] investigated the scattering of water waves by a surface-piercing thin vertical elastic plate using Green's function method. The time-dependent version of this problem was solved by Peter and Meylan [30] using a generalized eigenfunction expansion. Chakraborty and Mandal [5] employed the method described by Meylan [27] to study the scattering of water waves by a thin vertical elastic plate submerged in both deep and finite-depth water. Additionally, Chakraborty et al. [6] explored the behaviour of elastic plates with both clamped and free ends, floating in deep water or water of uniform finite depth, using the hypersingular integral equation method.

To enhance the environmental friendliness of vertical breakwaters, rigid vertical structures can be replaced with porous barriers placed at various positions in the ocean. Sollitt and Cross [43] initially studied the effect of barrier permeability on incident surface waves and modified Darcy's law, which many researchers later used in the field of porous breakwaters. Macaskill [23] solved the problem of normally incident wave scattering involving a permeable thin barrier in water of infinite depth by reducing it to integro-differential equations using Green's integral theorem. Chwang [7] developed a porous wavemaker theory to investigate the propagation of surface waves by the horizontal oscillation of a vertical porous plate. Yu [48] applied an

https://doi.org/10.1017/S1446181124000257 Published online by Cambridge University Press

approximate method to solve the problem of diffraction of surface water waves by a semi-infinite porous breakwater using a boundary condition based on Sollitt and Cross [43]. Isaacson et al. [15] used a matched eigenfunction expansion method to develop numerical solutions for the interaction of normally incident waves with a surface-piercing porous barrier and verified their results experimentally. Karmakar and Soares [17] investigated wave scattering by multiple bottom-standing flexible porous barriers using both the direct method and the wide-spacing approximation. Gayen and Mondal [11] explored the scattering of small-amplitude surface water waves by two symmetric vertical thin porous plates using the collocation method. Li et al. [20] developed an accurate solution to water wave scattering by porous barriers of different structures, including surface-piercing and bottom-standing barriers, using a multi-term Galerkin approximation. Manam and Sivanesan [24] used an analytical approach to solve deepwater wave motion over surface-piercing or bottom-standing porous barriers. Behera and Ng [2] employed eigenfunction expansions to investigate oblique wave scattering by multiple bottom-standing flexible porous barriers near a rigid wall. Sasmal et al. [38] and Sasmal and De [34, 35, 37] studied the scattering of water waves by various configurations of multiple porous barriers extending to infinite depth in a series of works.

In many of the studies documented above which examine various barrier configurations, the barriers are generally considered to be either impermeable or permeable. Furthermore, hydroelasticity theories for structures like floating elastic plates of arbitrary shapes and disks have been widely studied and reviewed by researchers in recent years. For instance, Sturova [44] investigated the linear hydroelastic problem of periodic surface pressures acting on plates of arbitrary shapes. Hassan et al. [12] studied the problem of water wave interaction with a submerged elastic plate of negligible thickness by the eigenfunction-matching method. Zheng et al. [50] developed a semi-analytical model based on linear potential flow theory and an eigenfunction expansion method to study wave scattering by a floating porous elastic plate with an arbitrary shape. The interaction of water waves with submerged porous elastic disks was also investigated by Zheng et al. [51]. Liu et al. [21] developed new analytical solutions for oblique wave scattering by porous rubble-mound breakwaters and seawalls based on contour integrals without finding complex roots. Zheng et al. [52] further developed a theoretical model based on linear potential flow theory and an eigenfunction matching method to investigate wave scattering by multiple circular floating porous elastic plates. Smith et al. [42] investigated the problem of water-wave scattering by a semi-infinite submerged thin elastic plate, whether porous or non-porous, using the Wiener–Hopf technique. Ashok et al. [1] presented explicit solutions to the problem of scattering of normally incident waves by a submerged flexible porous thin plate. Surface gravity wave interaction with an articulated flexible submerged plate in the presence of lateral compressive force was investigated by Boral et al. [3]. The problem of water wave scattering by a vertical porous elastic plate completely submerged in water of infinite depth in the presence of surface tension at the free surface was investigated by Singh and Gayen [39]. Singh and Kaligatla [40]

https://doi.org/10.1017/S1446181124000257 Published online by Cambridge University Press

studied the combined effect of refraction-diffraction due to bottom topography on water wave scattering by a vertical flexible-porous structure by employing the Galerkin approximation method. Recently, Sasmal and De [36] investigated the scattering of water waves with multiple flexible porous barriers by employing the Galerkin approximation method.

This paper investigates the feasibility of integrating hydro elasticity into the analysis of surface gravity wave interactions with multiple flexible, porous plates of arbitrary lengths in infinitely deep water. The potential function is simplified into linear integral equations using the Havelock inversion formula, followed by a matching process. These equations are solved using a single-term Galerkin approximation. Numerical estimates for the reflection coefficient, energy dissipation and wave force coefficients are provided for various parameter values. The method's convergence and accuracy are validated by comparing our results with existing literature. The findings indicate that the flexural rigidity of the porous plates significantly affects wave reflection, energy dissipation and wave forces. Moreover, the wave load decreases substantially as the number of plates increases.

2. Mathematical model

Here, we consider N number of porous elastic plates. Cartesian coordinate axes are chosen with the x-axis directed along the mean water surface, taking the y-axis vertically downwards. It is assumed that N number of unequal poroelastic plates are placed vertically, as shown in Figure 1. The jth vertical poroelastic plate is situated at $x = a_j,\ y \in L_j \equiv (h_{2j-1}, h_{2j}),\ j = 1, 2, 3, \ldots, N$. For the convenience of study, the fluid region is divided into $N + 1$ subregions, namely,

$$\begin{gathered} R_1 \equiv (-\infty < x < a_1, 0 < y < \infty), \\ R_j \equiv (a_{j-1} < x < a_j, 0 < y < \infty), \quad j = 2, 3, \ldots, N, \\ R_{N+1} \equiv (a_N < x < \infty, 0 < y < \infty). \end{gathered}$$

We use $N + 1$ velocity potentials $\phi_j,\ j = 1, 2, 3, \ldots, N + 1$ for the $N + 1$ subregions and $\overline{L}_j \equiv (0, \infty) - L_j,\ j = 1, 2, 3, \ldots, N$ to denote the fluid area of gaps of plates. It is assumed that the fluid is inviscid, incompressible, and the motion irrotational and simple harmonic in time with angular frequency ω. Assuming linear theory, the time-harmonic motions of the fluid are described by the velocity potential $\Phi_j(x, y, z, t) = Re\{\phi_j(x, y)e^{i\nu z - i\omega t}\}$, where Re denotes the real part and ν is defined by $\nu = K \sin\theta$, where $K = \omega^2/g$, g being the acceleration due to gravity, and θ is the angle of the incident wave to the x-axis. The spatial velocity potential $\phi_j(x, y)$ for $j = 1, 2, 3, \ldots, N + 1$ in each sub-region satisfies the governing Helmholtz equations given by

$$(\nabla^2 - \nu^2)\phi_j = 0, \quad -\infty < x < \infty, \quad 0 < y < \infty, \tag{2.1}$$

https://doi.org/10.1017/S1446181124000257 Published online by Cambridge University Press

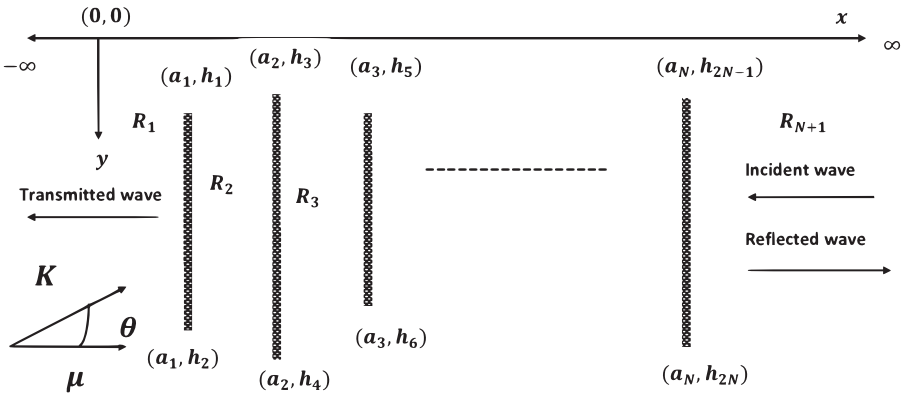

FIGURE 1. Schematic diagram of the physical domain demonstrating oblique scattering of surface gravity waves by an array of vertical flexible plates of arbitrary lengths.

where ∇^2 is the horizontal Laplacian operator and the subscript corresponds to the total wave field in each subregion.

The linearized kinematic and dynamic boundary conditions on the free surface can be merged into

$$\left(\frac{\partial}{\partial y} + K\right)\phi_j = 0 \quad \text{on } y = 0. \tag{2.2}$$

The no-flux boundary condition on the seabed is

$$|\nabla\phi_j| \to 0 \quad \text{as } y \to \infty, \tag{2.3}$$

where $\nabla = (\partial/\partial x, \partial/\partial y)$.

The plate is deflected horizontally with the displacement $\eta_j(y,t) = Re[v_j(y)e^{(-1)^j i\omega t}]$, $j = 1, 2, 3 \ldots, N$, where $v_j(y)$, $j = 1, 2, 3, \ldots, N$ is the complex quantity whose absolute value is assumed to be small. The conditions on the porous plates are given by (see the paper by Ashok et al. [1])

$$\frac{\partial\phi_j}{\partial x} = \frac{\partial\phi_{j+1}}{\partial x} = -iKG_j(\phi_{j+1} - \phi_j) - i\omega v_j(y), \quad x = x_j, \quad y \in L_j, \; j = 1, 2, 3, \ldots, N, \tag{2.4}$$

where $G_j = G_j^r + iG_j^i$, $j = 1, 2, 3, \ldots, N$ are the dimensionless porous effect parameters of poroelastic plates. The complex porous effect parameters can be written as [49]

$$G_j = \frac{\varepsilon_j(f_j + iS_j)}{K\alpha_j(f_j^2 + S_j^2)},$$

in which ε_j are the porosity constant, f_j are the resistance force coefficient, S_j are the inertial force coefficient and α_j are the thickness of the porous medium. The real part G_j^r represents the resistance effect of the porous material against the flow, while the imaginary part G_j^i represents the inertia effect of the fluid inside the porous material.

https://doi.org/10.1017/S1446181124000257 Published online by Cambridge University Press

The displacement amplitude $v_j(y),\ j = 1, 2, 3, \ldots, N$ satisfies (see [1])

$$\frac{\partial^4 v_j}{\partial y^4} - \lambda^2 v_j = -\frac{i\omega\rho}{EI}(\phi_{j+1} - \phi_j), \quad y \in L_j,\ j = 1, 2, 3, \ldots, N, \tag{2.5}$$

where $\lambda = \omega\sqrt{m_b/EI}$, EI is uniform flexural rigidity of porous barrier, m_b is uniform mass per unit length and ρ is the density of water.

In the vicinity of sharp submerged edges, the velocity potential behaves as [18, 25]

$$|\nabla\phi_j| = O(r^{-1/2}) \quad \text{as } r \to 0, \tag{2.6}$$

where $r = \sqrt{(x - a_j)^2 + (y - h)^2}$, where $h = h_{2j-1}, h_{2j},\ j = 1, 2, 3, \ldots, N$.

The conditions at infinity are given by

$$\begin{aligned} &\phi_1(x, y) = T\phi^{inc}(x, y) \quad \text{as } x \to -\infty, \\ &\phi_{N+1}(x, y) = \phi^{inc}(x, y) + R\phi^{inc}(-x, y) \quad \text{as } x \to \infty, \end{aligned} \tag{2.7}$$

where R and T are the unknown complex reflection and transmission coefficients to be determined, and $\phi^{inc}(x, y) = e^{-Ky - i\mu(x - a_N)}$, $\mu = K\cos\theta$.

At the common boundary of the region, velocity potential ϕ_j and gradient of velocity potential $\partial\phi_j/\partial x$ are continuous across the gap. Let us consider

$$f_j(y) = \frac{\partial\phi_j(a_j, y)}{\partial x} = \frac{\partial\phi_{j+1}(a_j, y)}{\partial x}, \quad \xi_j(y) = \phi_{j+1}(a_j, y) - \phi_j(a_j, y) \tag{2.8}$$

for $j = 1, 2, 3, \ldots, N$. Eliminating $v_j(y),\ j = 1, 2, 3, \ldots, N$, from (2.4) and (2.5) along with (2.8),

$$\begin{aligned} \left(\frac{\partial^4}{\partial y^4} - \lambda^2\right)\frac{\partial\phi_j}{\partial x} &= \left(\frac{\partial^4}{\partial y^4} - \lambda^2\right)\frac{\partial\phi_{j+1}}{\partial x} \\ &= -iKG_j\frac{\partial^4\xi_j(y)}{\partial y^4} + \lambda^2\left(iKG_j - \frac{\rho}{m_b}\right)\xi_j(y), \quad y \in L_j,\ j = 1, 2, 3, \ldots, N. \end{aligned} \tag{2.9}$$

3. Solution procedure

Applying the method of separation of variables, along with (2.1)–(2.7), Havelock's expansion of velocity potentials $\phi_j(x, y),\ j = 1, 2, 3, \ldots, N$ for each of the subregions is given by

$$\phi_1(x, y) = T\phi^{inc}(x, y) + \int_0^\infty A(k)e^{\zeta(x - a_1)}(k\cos ky - K\sin ky)\,dk \quad \text{in } R_1, \tag{3.1}$$

$$\begin{aligned} \phi_j(x, y) &= e^{-Ky}(c_j e^{i\mu x} + d_j e^{-i\mu x}) \\ &\quad + \int_0^\infty \{M_j(k)e^{-\zeta x} + N_j(k)e^{\zeta x}\}(k\cos ky - K\sin ky)\,dk \quad \text{in } R_j,\ j = 2, 3, \ldots, N, \end{aligned} \tag{3.2}$$

https://doi.org/10.1017/S1446181124000257 Published online by Cambridge University Press

$$\phi_{N+1}(x,y) = \phi^{inc}(x,y) + R\phi^{inc}(-x,y) + \int_0^\infty B(k)e^{-\zeta(x-a_N)}(k\cos ky - K\sin ky)\,dk \quad \text{in } R_{N+1}, \tag{3.3}$$

where $\zeta = \sqrt{k^2+\nu^2}$, and c_j, d_j are arbitrary constants, and $A(k)$, $B(k)$, $M_j(k)$, $N_j(k)$, $j = 2,3,\ldots,N$ are unknown functions and, in the mathematical analysis below in which they appear, are convergent.

Now, using the expression of velocity potentials ϕ_j from (3.1)–(3.3) in (2.8) and applying Havelock's inversion formula,

$$-Te^{-i\mu(a_1-a_N)} = c_2e^{i\mu a_1} - d_2e^{-i\mu a_1}, \quad -1 + Re^{2i\mu a_N} = c_Ne^{i\mu a_N} - d_Ne^{-i\mu a_N}, \tag{3.4}$$

$$c_je^{i\mu a_j} - d_je^{-i\mu a_j} = c_{j+1}e^{i\mu a_j} - d_{j+1}e^{-i\mu a_j}, \quad j = 2,3,\ldots,N-1, \tag{3.5}$$

$$A(k) = N_2(k)e^{\zeta a_1} - M_2(k)e^{-\zeta a_1}, \quad B(k) = N_N(k)e^{\zeta a_N} - M_N(k)e^{-\zeta a_N}, \tag{3.6}$$

$$N_j(k)e^{\zeta a_j} - M_j(k)e^{-\zeta a_j} = N_{j+1}(k)e^{\zeta a_j} - M_{j+1}(k)e^{-\zeta a_j}, \quad j = 2,3,\ldots,N-1, \tag{3.7}$$

$$-Te^{-i\mu(a_1-a_N)} + c_2e^{i\mu a_1} + d_2e^{-i\mu a_1} = 2K\int_{L_1} e^{-Ky}\xi_1(y)\,dy, \tag{3.8}$$

$$(c_{j+1}-c_j)e^{i\mu a_j} + (d_{j+1}-d_j)e^{-i\mu a_j} = 2K\int_{L_j} e^{-Ky}\xi_j(y)\,dy, \quad j = 2,3,\ldots,N-1, \tag{3.9}$$

$$1 + Re^{2i\mu a_N} - c_Ne^{i\mu a_N} - d_Ne^{-i\mu a_N} = 2K\int_{L_N} e^{-Ky}\xi_N(y)\,dy, \tag{3.10}$$

$$M_2(k)e^{-\zeta a_1} + N_2(k)e^{\zeta a_1} - A(k) = \frac{2}{\pi(k^2+K^2)}\int_{L_1}\xi_1(y)(k\cos ky - K\sin ky)\,dy, \tag{3.11}$$

$$(M_{j+1}(k) - M_j(k))e^{-\zeta a_j} + (N_{j+1}(k) - N_j(k))e^{\zeta a_j} = \frac{2}{\pi(k^2+K^2)}\int_{L_j}\xi_j(y)(k\cos ky - K\sin ky)\,dy, \; j = 2,3\ldots,N-1, \tag{3.12}$$

$$B(k) - M_N(k)e^{-\zeta a_N} - N_N(k)e^{\zeta a_N} = \frac{2}{\pi(k^2+K^2)}\int_{L_N}\xi_N(y)(k\cos ky - K\sin ky)\,dy. \tag{3.13}$$

Equations (3.8)–(3.10) can be reconstructed using the expressions from (3.4) and (3.5) as

$$2K\int_{L_1}\xi_1(y)e^{-Ky}\,dy = (i\cot(\mu(a_1-a_2)) - 1)Te^{-i\mu(a_1-a_N)} + i\csc(\mu(a_1-a_2))(c_2e^{i\mu a_2} - d_2e^{-i\mu a_2}), \tag{3.14}$$

$$2K\int_{L_2}\xi_2(y)e^{-Ky}\,dy = -i\csc(\mu(a_1-a_2))Te^{-i\mu(a_1-a_N)} + i\sin(\mu(a_3-a_1))\csc(\mu(a_3-a_2)) \times \csc(\mu(a_2-a_1))(c_2e^{i\mu a_2} - d_2e^{-i\mu a_2}) - i\csc(\mu(a_3-a_2))(c_3e^{i\mu a_3} - d_3e^{-i\mu a_3}), \tag{3.15}$$

https://doi.org/10.1017/S1446181124000257 Published online by Cambridge University Press

$$2K\int_{L_j}\xi_j(y)e^{-Ky}\,dy = -i\csc(\mu(a_j-a_{j-1}))(c_{j-1}e^{i\mu a_{j-1}}-d_{j-1}e^{-i\mu a_{j-1}})$$
$$+\,i\sin(\mu(a_{j+1}-a_{j-1}))\csc(\mu(a_j-a_{j-1}))\csc(\mu(a_{j+1}-a_j))(c_je^{i\mu a_j}-d_je^{-i\mu a_j})$$
$$-\,i\csc(\mu(a_{j+1}-a_j))(c_{j+1}e^{i\mu a_{j+1}}-d_{j+1}e^{-i\mu a_{j+1}}),\ j=3,4,\ldots,N-2, \tag{3.16}$$

$$2K\int_{L_{N-1}}\xi_{N-1}(y)e^{-Ky}\,dy = -i\csc(\mu(a_{N-1}-a_{N-2}))(c_{N-2}e^{i\mu a_{N-2}}-d_{N-2}e^{-i\mu a_{N-2}})$$
$$+\,i\sin(\mu(a_N-a_{N-2}))\csc(\mu(a_{N-1}-a_{N-2}))\csc(\mu(a_N-a_{N-1}))$$
$$\times(c_{N-1}e^{i\mu a_{N-1}}-d_{N-1}e^{-i\mu a_{N-1}})-i\csc(\mu(a_N-a_{N-1}))(1-Re^{2i\mu a_N}), \tag{3.17}$$

$$2K\int_{L_N}\xi_N(y)e^{-Ky}\,dy = -i\csc(\mu(a_N-a_{N-1}))(c_{N-1}e^{i\mu a_{N-1}}-d_{N-1}e^{-i\mu a_{N-1}})$$
$$+\,1-i\cot(\mu(a_N-a_{N-1}))+(1+i\cot(\mu(a_N-a_{N-1})))Re^{2i\mu a_N}. \tag{3.18}$$

Substituting the expressions of $A(k)$, $B(k)$, $M_j(k)$, $N_j(k)$, $j=2,3,\ldots,N$ from (3.11)–(3.13) after using the relation of (3.6) and (3.7) in (2.9),

$$\sum_{m=1}^{N}\int_{L_m}\xi_m(t)\mathcal{H}_{nm}(y,t)dt+\mathcal{E}\xi_n(y)=S_n(y),\quad n=1,2,3,\ldots,N, \tag{3.19}$$

where

$$\mathcal{E}=\lambda^2(iKG_n-\rho/m_b)/(K^4-\lambda^2);$$
$$S_1(y)=-i\mu Te^{i\mu(a_N-a_1)-Ky};\quad S_N(y)=-i\mu e^{-Ky}(1-Re^{2i\mu a_N});$$
$$S_j(y)=i\mu e^{-Ky}(c_je^{i\mu a_j}-d_je^{-i\mu a_j}),\quad j=2,3,\ldots,N-1,$$

and

$$\begin{cases}\mathcal{H}_{nn}(y,t)=-\dfrac{2iK^6G_n}{(K^4-\lambda^2)}e^{-K(y+t)}+\dfrac{1}{\pi(K^4-\lambda^2)}\\ \quad\times\displaystyle\int_0^\infty\left(\frac{\zeta(k^4-\lambda^2)}{k^2+K^2}-\frac{2iKG_nk^4}{k^2+K^2}\right)(k\cos ky-K\sin ky)(k\cos kt-K\sin kt)\,dk,\\ \mathcal{H}_{mn}(y,t)=\mathcal{H}_{nm}(y,t)=\dfrac{1}{\pi(K^4-\lambda^2)}\\ \quad\times\displaystyle\int_0^\infty\frac{\zeta(k^4-\lambda^2)}{k^2+K^2}e^{\zeta(a_m-a_n)}(k\cos ky-K\sin ky)(k\cos kt-K\sin kt)\,dk;\\ m,n=1,2,\ldots,N.\end{cases} \tag{3.20}$$

Let us consider potential difference function $\xi_m(t)$ as

$$\xi_m(t)=-i\mu Te^{i\mu(a_N-a_1)}X_{m1}(t)-i\mu(1-Re^{2i\mu a_N})X_{mN}(t)$$
$$+\,i\mu\sum_{j=2}^{N-1}(c_je^{i\mu a_j}-d_je^{-i\mu a_j})X_{mj}(t),m=1,2,3,\ldots,N. \tag{3.21}$$

https://doi.org/10.1017/S1446181124000257 Published online by Cambridge University Press

After using the expressions of $g_m(t)$ from (3.21), the integral equations in (3.19) can be reduced as

$$\sum_{m=1}^{N}\int_{L_m} X_{mj}(t)\mathcal{H}_{nm}(y,t)\,dt + \mathcal{E}X_{nj}(y) = \delta_{nj}e^{-Ky}, y \in L_n, n, \quad j = 1,2,3,\ldots,N, \quad (3.22)$$

where δ_{nj} is the Kronecker delta symbol.

3.1. Solutions of integral equations using Galerkin's approximation technique

The integral equations given by (3.22) have been solved using the single-term Galerkin technique. The unknown functions $X_{ij}(y)$ are chosen in the following form:

$$X_{mj}(t) = b_{mj}\,\mathcal{F}_m(t), \quad m,j = 1,2,3,\ldots,N, \quad (3.23)$$

where $\mathcal{F}_j(t)$ are suitably chosen basis functions and b_{mj}, unknown constants, are to be found.

To deduce the unknown constants b_{mj} appearing in (3.23), we substitute the expressions of $X_{mj}(t)\,(m,j = 1,2,3,\ldots,N)$ from (3.23) into the integral equations in (3.22), then multiply the mth integral equation in (3.22) by $\mathcal{F}_m(t)$ and integrate over L_m. This yields the following linear systems of equations in $b_{mj}\,(m,j = 1,2,3,\ldots,N)$:

$$\sum_{m=1}^{N} b_{mj}\mathcal{C}_{nm} = \delta_{nj}\mathcal{D}_n, \quad n,j = 1,2,3,\ldots,N, \quad (3.24)$$

where

$$\begin{cases} \mathcal{C}_{nn} = \displaystyle\int_{L_n}\mathcal{F}_n(y)\Big\{\int_{L_n}\mathcal{F}_n(t)\mathcal{H}_{nn}(y,t)\,dt\Big\}dy + \mathcal{E}\int_{L_n}[\mathcal{F}_n(y)]^2\,dy, \\ \mathcal{C}_{nm} = \mathcal{C}_{mn} = \displaystyle\int_{L_n}\mathcal{F}_n(y)\Big\{\int_{L_m}\mathcal{F}_m(t)\mathcal{H}_{nm}(y,t)\,dt\Big\}dy, \quad n \neq m, \\ \mathcal{D}_n = \displaystyle\int_{L_n}\mathcal{F}_n(y)e^{-ky}\,dy, \quad n,m = 1,2,3,\ldots,N. \end{cases} \quad (3.25)$$

We choose the basis function $\mathcal{F}_m(y), m = 1,2,3,\ldots,N$ as follows (see [40]):

$$\mathcal{F}_m(y) = e^{-Ky}\Big[\int_{h_{2m-1}}^{y}\frac{(d_m^2 - z^2)e^{Kz}}{\sqrt{(z^2 - h_{2m-1}^2)(h_{2m}^2 - z^2)}}\,dz\Big], \quad h_{2m-1} < y < h_{2m}, \quad (3.26)$$

where

$$d_m^2 = \frac{\displaystyle\int_{h_{2m-1}}^{h_{2m}}\frac{z^2e^{Kz}}{\sqrt{(z^2-h_{2m-1}^2)(h_{2m}^2-z^2)}}\,dz}{\displaystyle\int_{h_{2m-1}}^{h_{2m}}\frac{e^{Kz}}{\sqrt{(z^2-h_{2m-1}^2)(h_{2m}^2-z^2)}}\,dz}, \quad m = 1,2,3,\ldots,N.$$

https://doi.org/10.1017/S1446181124000257 Published online by Cambridge University Press

Substituting the expressions of $\mathcal{F}_m(y)$ from (3.26) and $\mathcal{H}_{mn}(y,t)$ from (3.20) into (3.25),

$$C_{nn} = \frac{1}{\pi(K^4-\lambda^2)}\int_0^\infty \left(\frac{\zeta(k^4-\lambda^2)}{k^2+K^2} - \frac{2iKG_nk^4}{k^2+K^2}\right)\left[\int_{h_{2n-1}}^{h_{2n}} \frac{(d_n^2-z^2)\sin kz}{\sqrt{(z^2-h_{2n-1}^2)(h_{2n}^2-z^2)}}\,dz\right]^2 dk$$
$$- \frac{iK^4G_n}{2(K^4-\lambda^2)}\left[\int_{h_{2n-1}}^{h_{2n}} \frac{(d_n^2-z^2)e^{-Kz}}{\sqrt{(z^2-h_{2n-1}^2)(h_{2n}^2-z^2)}}\,dz\right]^2 + \frac{\lambda^2(iKG_n-\frac{\rho}{m_b})}{K^4-\lambda^2}$$
$$\times \int_{h_{2n-1}}^{h_{2n}} e^{-2Kt}\left[\int_{h_{2n-1}}^{t} \frac{(d_n^2-z^2)e^{Kz}}{\sqrt{(z^2-h_{2n-1}^2)(h_{2n}^2-z^2)}}\,dz\right]^2 dt, \quad n=1,2,3,\ldots,N,$$

$$C_{mn} = C_{nm} = \frac{1}{\pi(K^4-\lambda^2)}\int_0^\infty \frac{\zeta(k^4-\lambda^2)e^{\zeta(a_m-a_n)}}{k^2+K^2}\left[\int_{h_{2m-1}}^{h_{2m}} \frac{(d_m^2-z^2)\sin kz}{\sqrt{(z^2-h_{2m-1}^2)(h_{2m}^2-z^2)}}\,dz\right]$$
$$\times\left[\int_{h_{2n-1}}^{h_{2n}} \frac{(d_n^2-z^2)\sin kz}{\sqrt{(z^2-h_{2n-1}^2)(h_{2n}^2-z^2)}}\,dz\right]dk, \quad m,n=1,2,3,\ldots N,$$

$$\mathcal{D}_n = \frac{1}{2K}\int_{h_{2n-1}}^{h_{2n}} \frac{(d_n^2-z^2)e^{Kz}}{\sqrt{(z^2-h_{2n-1}^2)(h_{2n}^2-z^2)}}\,dz, \quad n=1,2,3,\ldots,N.$$

3.2. Determination of reflection and transmission coefficients To determine the coefficients R and T, we substitute the expression from (3.21) into (3.14)–(3.18), then these equations can be written in the matrix notation as

$$(P+Q)V = W, \tag{3.27}$$

where

$$Q = \begin{bmatrix} i+\cot(\mu(a_1-a_2)) & -\csc(\mu(a_1-a_2)) & - & - & - & - & - & 0 \\ -\csc(\mu(a_1-a_2)) & \sin(\mu(a_3-a_1))\csc(\mu(a_3-a_2))\csc(\mu(a_2-a_1)) & - & - & - & - & - & 0 \\ - & - & - & - & - & - & - & - \\ - & - & - & - & - & - & - & - \\ - & - & - & - & - & - & - & - \\ 0 & - & - & - & - & - & - & \csc(\mu(a_N-a_{N-1})) \\ 0 & 0 & - & - & - & - & - & i-\cot(\mu(a_N-a_{N-1})) \end{bmatrix},$$

$$V = \begin{bmatrix} -Te^{i\mu(a_N-a_1)} \\ (c_2e^{i\mu a_2}-d_2e^{-i\mu a_2}) \\ - \\ - \\ - \\ - \\ (c_{N-1}e^{i\mu a_{N-1}}-d_{N-1}e^{-i\mu a_{N-1}}) \\ Re^{2i\mu a_N} \end{bmatrix}, \quad W = \begin{bmatrix} 2K\mu P_{1N} \\ 2K\mu P_{2N} \\ - \\ - \\ - \\ - \\ 2K\mu P_{(N-1)N}+\csc(\mu(a_N-a_{N-1})) \\ 2K\mu P_{NN}-i-\cot(\mu(a_N-a_{N-11})) \end{bmatrix},$$

https://doi.org/10.1017/S1446181124000257 Published online by Cambridge University Press

$$P = 2K\mu \begin{bmatrix} P_{11} & P_{12} & - & - & - & - & P_{1N} \\ P_{21} & P_{22} & - & - & - & - & P_{2N} \\ - & - & - & - & - & - & - \\ - & - & - & - & - & - & - \\ P_{N1} & P_{N2} & - & - & - & - & P_{NN} \end{bmatrix},$$

with $P_{mj} = \int_{L_m} X_{mj}(t)e^{-Kt}\,dt$, $m, j = 1, 2, 3, \ldots, N$. Once the unknown constants $b_{mj}, m, j = 1, 2, 3, \ldots, N$ are obtained after solving the system of equations (3.24), then $X_{mj}, m, j = 1, 2, 3, \ldots, N$ from relations of (3.23) can be obtained. Hence, R and T can be determined by solving (3.27).

3.3. Dynamic wave force The dynamic pressure $P(x, y)$ can be obtained according to the Bernoulli equation (see [20, 39]),

$$P(x, y) = -i\rho\omega \sum_{j=1}^{N} \xi_j(y).$$

The magnitude of horizontal wave force acting on plates can be obtained by integrating the dynamic pressure along the porous plates as follows [20, 39]:

$$C_f = -i\rho\omega \sum_{j=1}^{N} \int_{L_j} \xi_j(y)\,dy.$$

The nondimensional form of the horizontal force coefficient on the vertical porous plates is given by

$$K_f = \frac{K\,|C_f|}{\rho g}.$$

3.4. Energy identity relation The energy identity plays an important role in the theoretical study of water wave scattering by plates. Some of the incident wave energy can be dissipated by the porous plates. The absolute values of the reflection and transmission coefficients are connected by the relation (see [39])

$$|R|^2 + |T|^2 = 1 - J. \tag{3.28}$$

Here, J signifies the amount of dissipated energy due to the permeability of plates and its expression in terms of the potential differences across the plates is found to be (see [39])

$$J = \frac{2K^2}{\mu} \sum_{j=1}^{N} G_j^r \int_{L_j} |\xi_j(y)|^2\,dy,$$

where G_j^r is the real part of the porous effect parameters. It is noticed from the expression of J that the integrand in the right-hand side of (3.28) is always positive for a nonzero G_j^r so that $|R|^2 + |T|^2 < 1$ for the case of permeable barriers, whereas for impermeable plates, the energy identity relation satisfy $|R|^2 + |T|^2 = 1$, which provides the convergence of result in the present study.

https://doi.org/10.1017/S1446181124000257 Published online by Cambridge University Press

TABLE 1. Values of $|R|$, $|T|$, $|R|^2+|T|^2$ and $1-J$ against KH_2 with $x_1=0.5, x_2=1.5, x_3=2.5, x_4=3.5, E=0.4, M=0.01, G_1=G_2=G_3=G_4=1, H_1=H_3=H_5=H_7=0.05, H_4=H_6=H_8=1, \theta=45^\circ$.

KH_2	$\lvert R\rvert$	$\lvert T\rvert$	$\lvert R\rvert^2+\lvert T\rvert^2$	$1-J$
0.100	0.000206133	0.999998	1	1
0.385	0.004231140	0.999991	0.99999935	0.9999950
0.670	0.136105000	0.990694	0.99999915	0.9998059
0.955	0.311106000	0.950375	0.99999975	0.9971371
1.240	0.677203000	0.735796	0.99999934	0.9912569

TABLE 2. Values of $|R|$, $|T|$ and $|R|^2+|T|^2$ against KH_2 with $x_1=0.5, x_2=1.5, x_3=2.5, x_4=3.5, E=0.4, M=0.01, G_1=G_2=G_3=G_4=0, H_1=H_3=H_5=H_7=0.05, H_4=H_6=H_8=1, \theta=45^\circ$.

KH_2	$\lvert R\rvert$	$\lvert T\rvert$	$\lvert R\rvert^2+\lvert T\rvert^2$
0.100	0.00286705	0.999996	1.0000
0.385	0.00671552	0.999977	1.0000
0.670	0.30467700	0.952456	1.0000
0.955	0.34799000	0.937498	1.0000
1.240	0.80539100	0.592744	1.0000

TABLE 3. Values of $|J|$ against KH_2 with $E=0.4, M=0.01, \theta=45^\circ$ and $G_N=1 (N=1,2,\ldots,6)$.

KH_2	$\lvert J\rvert(N=1)$	$\lvert J\rvert(N=2)$	$\lvert J\rvert(N=3)$	$\lvert J\rvert(N=4)$	$\lvert J\rvert(N=5)$	$\lvert J\rvert(N=6)$
0.10	0.0000000003	0.0000000027	0.0000000152	0.0000000182	0.0000000298	0.0000000345
0.45	0.0000451634	0.0000996050	0.0001797899	0.0003535529	0.0004334520	0.0006272150
0.80	0.0028337400	0.0060043800	0.0120460000	0.0144364000	0.0184780200	0.0198684200
1.15	0.0351156000	0.0554706000	0.0707459000	0.1043440000	0.1196193000	0.1532174000
1.50	0.0994097000	0.2403220000	0.2901240000	0.3854800000	0.4352820000	0.4936380000

For different values of KH_2, the above relations (3.28) and $|R|^2+|T|^2=1$ can be verified as in the last column of Tables 1 and 2 which certainly gives a partial check on the validation of the problem studied here for $N=4$. Table 1 represents the set of values $|R|$, $|T|$, $|R|^2+|T|^2$ and $1-J$ as a function of the wave number KH_2 for the case of porous plates. Table 2 shows $|R|$ and $|T|$, and that $|R|^2+|T|^2$ satisfies the energy identity for impermeable plates. These two tables imply the convergence of the numerical results obtained in the present manuscript. Table 3 represents the amount of dissipated energy $|J|$ for the different number of plates. It is observed that $|J|$ increases monotonically as KH_2 increases, regardless of the number of plates included in the array. Additionally, Table 3 shows that arrays containing more plates lead to larger values of $|J|$ for the whole computed range of wave conditions. This suggests that the use of multiple plates can be more effective in dissipating wave energy.

https://doi.org/10.1017/S1446181124000257 Published online by Cambridge University Press

4. Results and discussion

In this section, the characteristics of arbitrary poroelastic plates are demonstrated in attenuating wave forces and dissipating wave energy through numerous results. The numerical results are calculated assuming $N = 4$ for four poroelastic plates. The numerical results are plotted for the reflection coefficient, the transmission coefficient, the total energy and the deflection of the structure. Consider the dimensionless parameters $M = m_b/\rho h_2$, $E = EI/\rho g h_2^4$ for the elastic porous plates. All results are presented versus the nondimensional frequency, which is defined as KH_2. The parametric values that are kept constant throughout the numerical computations are given by fluid density $\rho = 1025.0$ kg/m^3 and $g = 9.81$ m/s^2. The nondimensional parameters are given as

$$x_j = \frac{a_j}{h_2},\ j = 1,2,3,4; \quad H_j = \frac{h_j}{h_2},\ j = 1,2,8; \quad d_j = x_j - x_{j-1},\ j = 2,3,4.$$

4.1. Model validation with existing results In this section, we compared the present results with known limiting cases when certain parameters are assumed to be absent. It helps validate theoretical models and computational methods. When specific parameters are neglected or set to zero, it induces significant alterations in the behaviour of structures, particularly evident in plate structures.

We verified the results for permeable plates obtained in this study by comparing them with those obtained by Gayen and Mondal [11], who employed the hypersingular integral equation method for analysing two equal plates. Gayen and Mondal [11] plotted $|R|$ against dimensionless wave number $K(d + b)(\equiv Kh_2$ in this study) for three different values of $\mu = (d - b)/(d + b)(\equiv H_1 = H_3$ in this study) while keeping the length of separation between plates, porosity and incident wave angle fixed in their figure 4. In this paper, we plotted $|R|$ against KH_2 for specific values: $x_1 = -0.3, x_2 = x_3 = x_4 = 0.3, H_4 = 1, G_1 = G_2 = 1, G_3 = G_4 = 0$, and $H_1 = H_3 = 0.01, 0.05, 0.25$ and $\theta = 0^o, M = 0.001, E = 0.999$ in Figure 2. It is observed that the corresponding curves from Gayen and Mondal [11] for two equal plates nearly coincide with those depicted in Figure 2. This comparison provides additional validation for our results and suggests agreement between the methodologies employed in both studies.

Finally, we assessed our solutions for a single elastic barrier by comparing them with numerical results derived from Green's function, as developed by Meylan [27]. For this comparison, we normalized the parameters and constructed Figure 3 for normal incident waves with a wavelength denoted by ς, where $\varsigma = 2\pi/K$, as was done by Meylan [27]. In Figure 3, we plotted the curves of $|R|$ against the depth of the plate $l(h_2/\varsigma)$ for various values of $E_1 \equiv (E/\varsigma)$ in the case of normal incident wave. The curves of Figure 3 almost coincide with those presented by Meylan [27]. This agreement further validates the accuracy and reliability of our method.

4.2. Effects of various parameters on results This subsection presents computed results for various parameter values of flexible porous plates. The accompanying graphs provide a visual representation of these findings.

https://doi.org/10.1017/S1446181124000257 Published online by Cambridge University Press

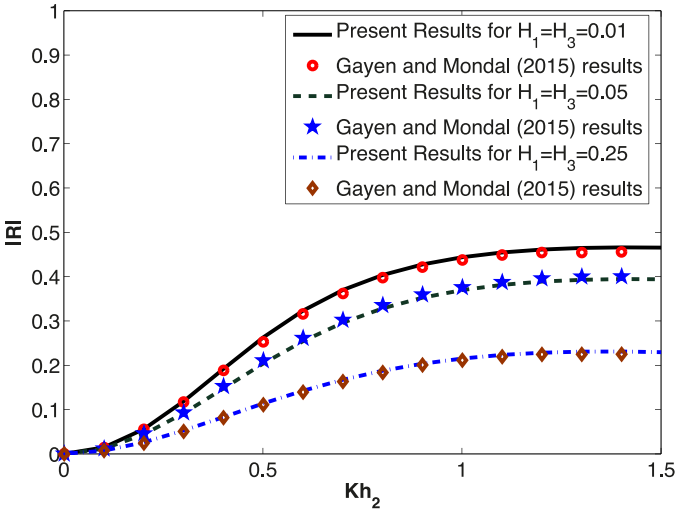

FIGURE 2. $|R|$ against KH_2 for $x_1 = -0.3, x_2 = x_3 = x_4 = 0.3, E = 0.999, M = 0.001, G_1 = G_2 = 1, G_3 = G_4 = 0, \theta = 0^o, H_4 = 1$.

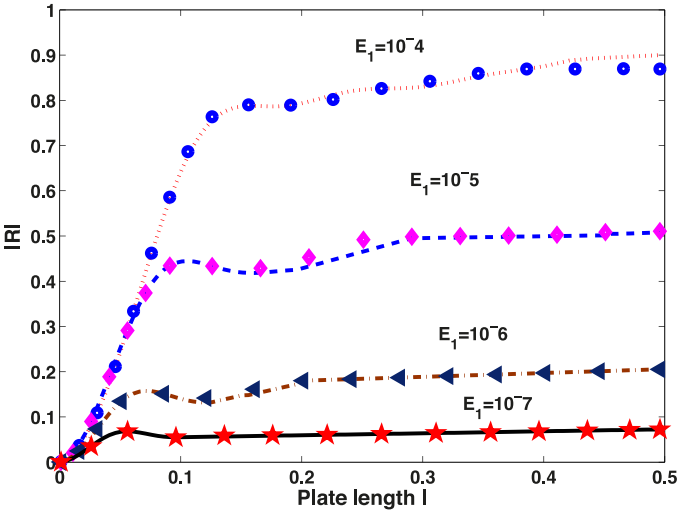

FIGURE 3. $|R|$ against depth of the plate $l(= h_2/\varsigma)$ for $a_1/\varsigma = a_2/\varsigma = a_3/\varsigma = a_4/\varsigma = 0, h_1/\varsigma = 0.001, M = 0.01, G_1 = G_2 = G_3 = G_4 = 0, \theta = 0^o, (E_1 \equiv (E/\varsigma))$.

Reflection coefficient $|R|$ is plotted against wave number KH_2 for the angle of incidence $\theta = 0°, 30°, 45°, 60°$ in Figures 4 and 5. The peak value of the reflection coefficient decreases as the angle of incidence increases. This trend is attributed to the mutual interaction between incident and reflected waves within the plates. The maximum and minimum values of $|R|$ shift from left to right as the angle of incidence

https://doi.org/10.1017/S1446181124000257 Published online by Cambridge University Press

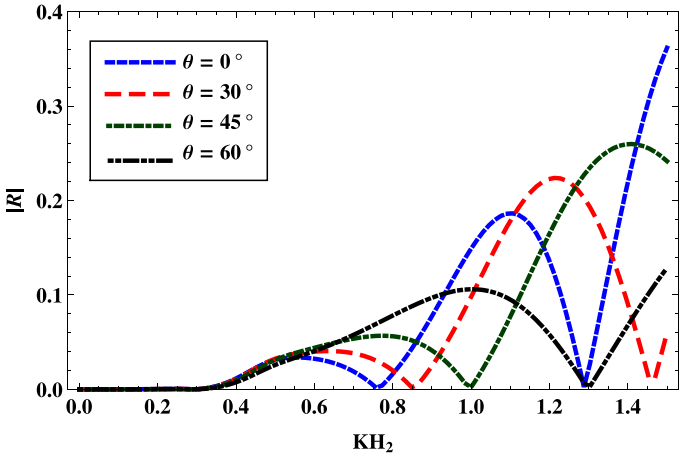

FIGURE 4. $|R|$ against KH_2 for $x_1 = 0.5, x_2 = 1.5, x_3 = 2.5, x_4 = 3.5, E = 0.4, M = 0.01, G_1 = G_2 = G_3 = G_4 = 1$, $H_1 = H_3 = H_5 = H_7 = 0.05, H_4 = H_6 = H_8 = 1$.

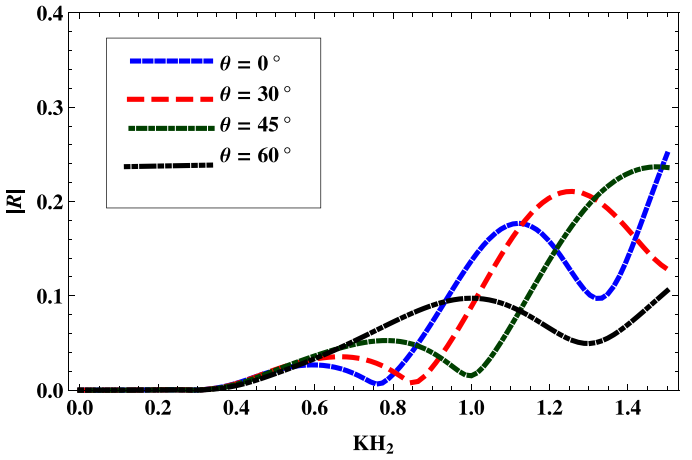

FIGURE 5. $|R|$ against KH_2 for $x_1 = 0.5, x_2 = 1.5, x_3 = 2.5, x_4 = 3.5, E = 0.4, M = 0.01, G_1 = 1, G_2 = 1.5$, $G_3 = 1.75, G_4 = 2, H_1 = H_3 = H_5 = H_7 = 0.05, H_4 = H_6 = H_8 = 1$.

increases. This shift suggests changes in the behaviour of reflected waves with varying angles of incidence. Comparing figures of equal and nonequal porosity, there is a significant increase in the maximum and minimum values of $|R|$ for equal porosity. This indicates that porosity influences the reflection properties of the plates, with equal porosity leading to higher reflection coefficients. The reflection coefficients exhibit an oscillatory nature for larger wave numbers. Moreover, higher oscillations are observed for smaller values of θ, indicating a dependence on the angle of incidence. From all these figures, we can conclude that the reflection coefficient tends to be small when the porosity is large.

https://doi.org/10.1017/S1446181124000257 Published online by Cambridge University Press

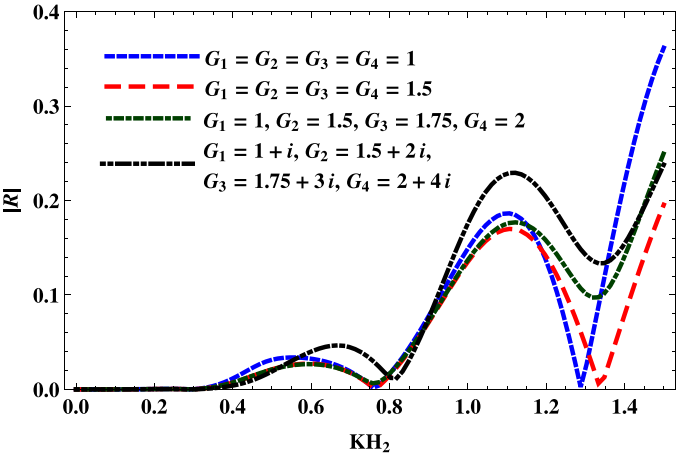

FIGURE 6. $|R|$ against KH_2 for $x_1 = 0.5, x_2 = 1.5, x_3 = 2.5, x_4 = 3.5, E = 0.4, M = 0.01, H_1 = H_3 = H_5 = H_7 = 0.05, H_4 = H_6 = H_8 = 1\theta = 0°$.

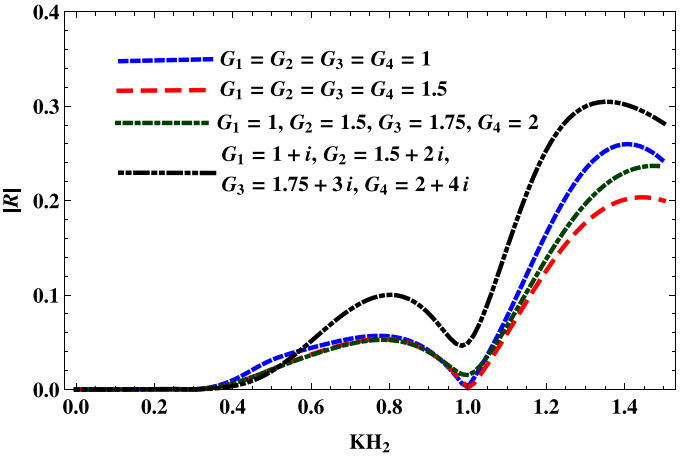

FIGURE 7. $|R|$ against KH_2 for $x_1 = 0.5, x_2 = 1.5, x_3 = 2.5, x_4 = 3.5, E = 0.4, M = 0.01, H_1 = H_3 = H_5 = H_7 = 0.05, H_4 = H_6 = H_8 = 1, \theta = 45°$.

Figures 6 and 7 depict the reflection coefficient $|R|$ versus the nondimensional wave number KH_2 for different porosity values. The figures illustrate how the reflection coefficient $|R|$ changes for four identical flexible plates subjected to normal and oblique incident waves. The minimum and maximum values of $|R|$ occur at specific wave numbers. However, as the porosity increases, the reflection coefficient $|R|$ decreases. This decrease is attributed to the increase in wave energy dissipation associated with higher porosity. The porous effect parameters influence the behaviour of the reflection coefficient. Similar to previous observations, the reflection coefficients exhibit an

https://doi.org/10.1017/S1446181124000257 Published online by Cambridge University Press

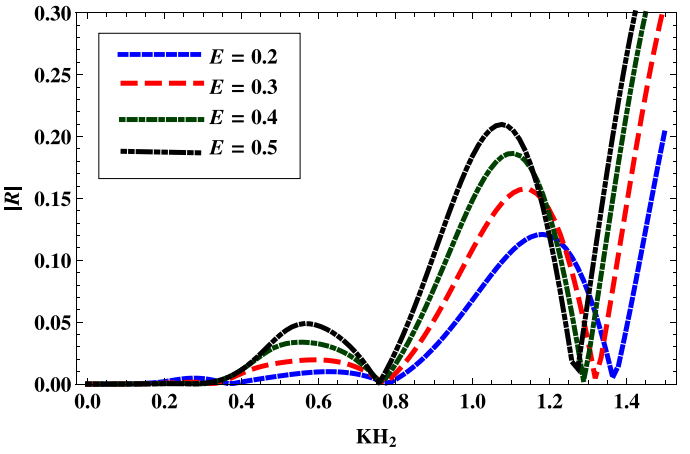

FIGURE 8. $|R|$ against KH_2 for $x_1 = 0.5, x_2 = 1.5, x_3 = 2.5, x_4 = 3.5, M = 0.01, G_1 = G_2 = G_3 = G_4 = 1$, $H_1 = H_3 = H_5 = H_7 = 0.05, H_4 = H_6 = H_8 = 1, \theta = 0°$.

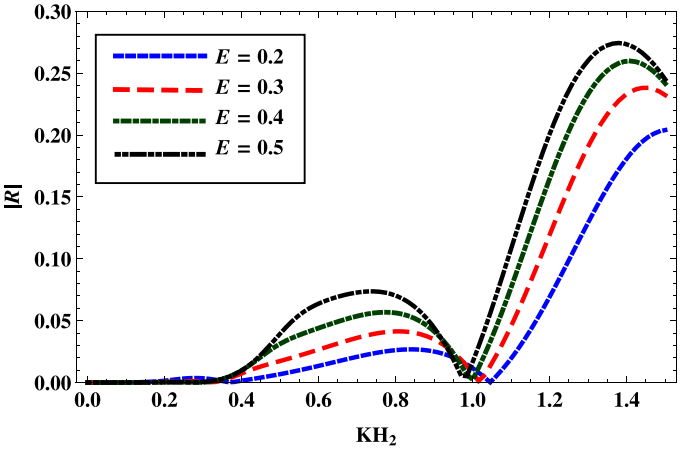

FIGURE 9. $|R|$ against KH_2 for $x_1 = 0.5, x_2 = 1.5, x_3 = 2.5, x_4 = 3.5, M = 0.01, G_1 = G_2 = G_3 = G_4 = 1$, $H_1 = H_3 = H_5 = H_7 = 0.05, H_4 = H_6 = H_8 = 1, \theta = 45°$.

oscillatory behaviour for larger wave numbers. This oscillation pattern is characteristic of the interaction between waves and the porous plates.

Figures 8–11 analyse the reflection coefficient $|R|$ versus the nondimensional wave number KH_2 for different values of flexural rigidity E. Figures 8 and 9 focus on the impact of flexural rigidity on $|R|$ involving equal plates with identical porosity, corresponding to normal and oblique incident waves, respectively. Figures 10 and 11 examine the influence of flexural rigidity on wave reflection under conditions of nonidentical porosity, covering both normal and oblique incident waves. The trend observed across all figures is that the values of $|R|$ increase as the flexural rigidity E

https://doi.org/10.1017/S1446181124000257 Published online by Cambridge University Press

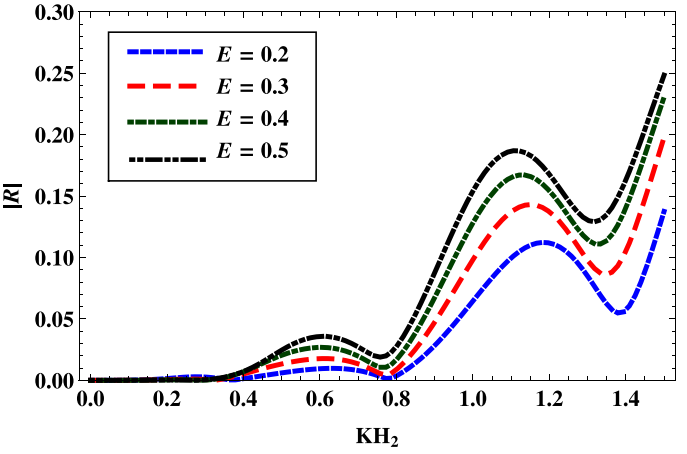

FIGURE 10. $|R|$ against KH_2 for $x_1 = 0.5, x_2 = 1.5, x_3 = 2.5, x_4 = 3.5, M = 0.01, G_1 = 1, G_2 = 1.5, G_3 = 2, G_4 = 2.5, H_1 = H_3 = H_5 = H_7 = 0.05, H_4 = H_6 = H_8 = 1, \theta = 0°$.

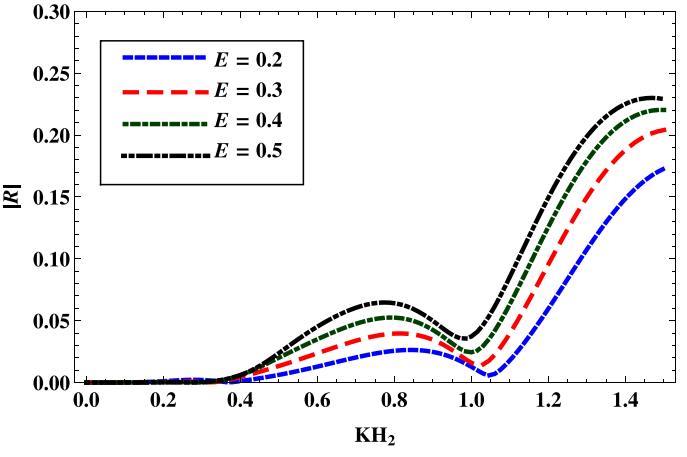

FIGURE 11. $|R|$ against KH_2 for $x_1 = 0.5, x_2 = 1.5, x_3 = 2.5, x_4 = 3.5, M = 0.01, G_1 = 1, G_2 = 1.5, G_3 = 2, G_4 = 2.5, H_1 = H_3 = H_5 = H_7 = 0.05, H_4 = H_6 = H_8 = 1, \theta = 45°$.

increases. This suggests that higher flexural rigidity enhances the reflection of waves when flexible porous plates are present. However, there is a notable difference in the peak values of $|R|$ between curves with equal and nonidentical porosity. In the case of nonidentical porosity, the peak values of $|R|$ are reduced compared with those with equal porosity. This indicates that variations in porosity between the plates influence the reflection characteristics, likely due to differences in how the waves interact with the plates.

Figures 12 and 13 provide an analysis of the reflection coefficients $|R|$ as a function of the nondimensional wave number KH_2 for various values of plate separation length.

https://doi.org/10.1017/S1446181124000257 Published online by Cambridge University Press

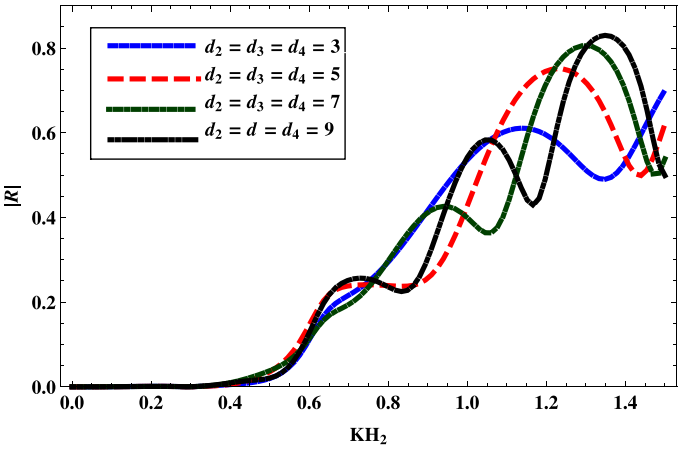

FIGURE 12. $|R|$ against KH_2 for $E = 0.4, M = 0.01, G_1 = G_2 = G_3 = G_4 = 1, H_1 = H_3 = H_5 = H_7 = 0.05$, $H_4 = H_6 = H_8 = 1, \theta = 0°$.

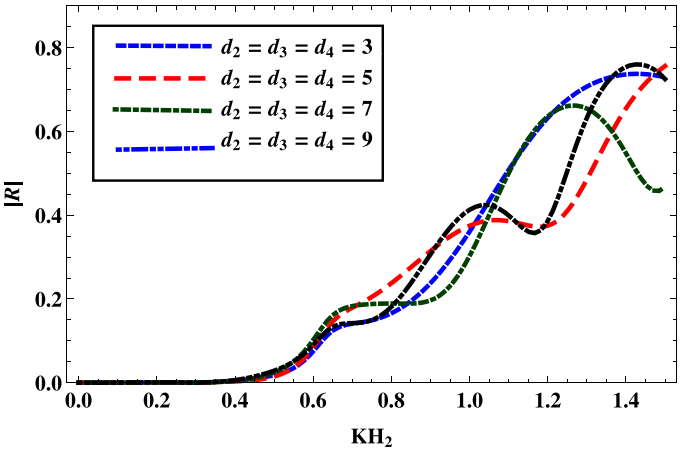

FIGURE 13. $|R|$ against KH_2 for $E = 0.4, M = 0.01, G_1 = G_2 = G_3 = G_4 = 1, H_1 = H_3 = H_5 = H_7 = 0.05$, $H_4 = H_6 = H_8 = 1, \theta = 45°$.

As the separation length between the plates decreases, the values of $|R|$ shift towards the right. This indicates a correlation between plate separation length and the position of the peak reflection coefficient. The peak value of $|R|$ is observed to decrease in the case of an oblique incident wave compared with a normal incident wave. Across all figures, the oscillation of $|R|$ increases as the plate's separation length increases. This phenomenon can be attributed to constructive and/or destructive interference between incident and reflected waves within the flexible porous plates.

The reflection coefficient $|R|$ is plotted against KH_2 for varying submergence depths of the plates in Figures 14 and 15, corresponding to normal and oblique incident

https://doi.org/10.1017/S1446181124000257 Published online by Cambridge University Press

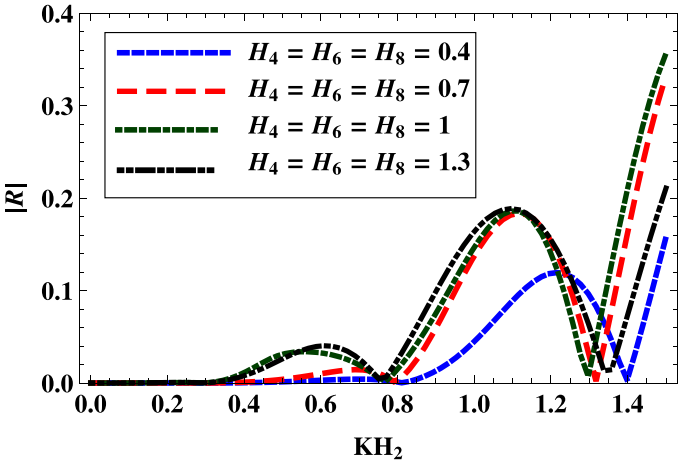

FIGURE 14. $|R|$ against KH_2 for $E = 0.4, M = 0.01, G_1 = G_2 = G_3 = G_4 = 1, H_1 = H_3 = H_5 = H_7 = 0.05$, $H_4 = H_6 = H_8 = 1, \theta = 0°$.

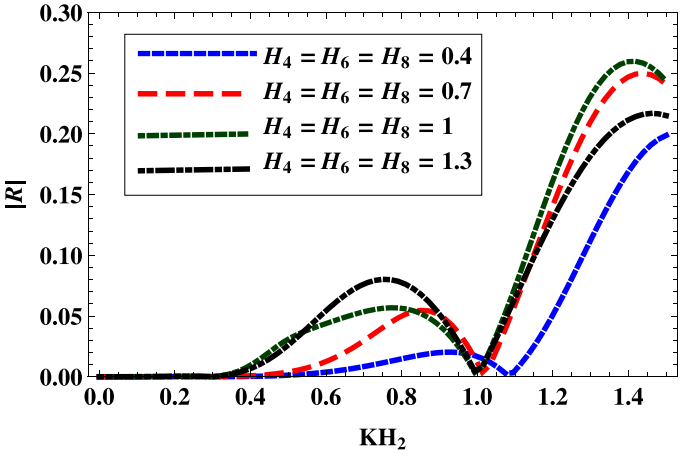

FIGURE 15. $|R|$ against KH_2 for $E = 0.4, M = 0.01, G_1 = G_2 = G_3 = G_4 = 1, H_1 = H_3 = H_5 = H_7 = 0.05$, $H_4 = H_6 = H_8 = 1, \theta = 0°$.

waves, respectively. It is noted that as the submergence depth of the plates decreases, the values of $|R|$ shift towards the right. Additionally, the peak value of $|R|$ is lower for oblique incident waves compared with normal incident waves. In the case of oblique incident waves, the overall reflection coefficient is generally lower across all submergence depths, highlighting the effect of wave direction on the interaction with submerged plates.

Figures 16 and 17 depict the dimensionless amplitudes of wave forces acting on plates plotted against the nondimensional wave number KH_2 for different values of the porous effect parameter. These figures provide insight into how the amplitude of wave

https://doi.org/10.1017/S1446181124000257 Published online by Cambridge University Press

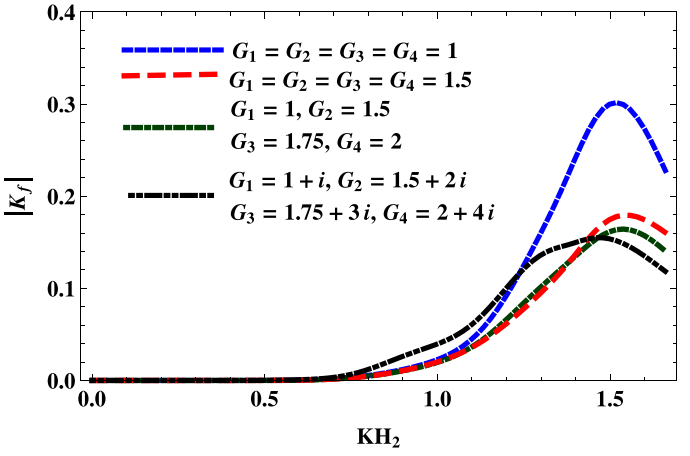

FIGURE 16. $|K_f|$ against KH_2 for $x_1 = 0.5, x_2 = 1.5, x_3 = 2.5, x_4 = 3.5, E = 0.4, M = 0.01, H_1 = H_3 = H_5 = H_7 = 0.05, H_4 = H_6 = H_8 = 1, \theta = 0°$.

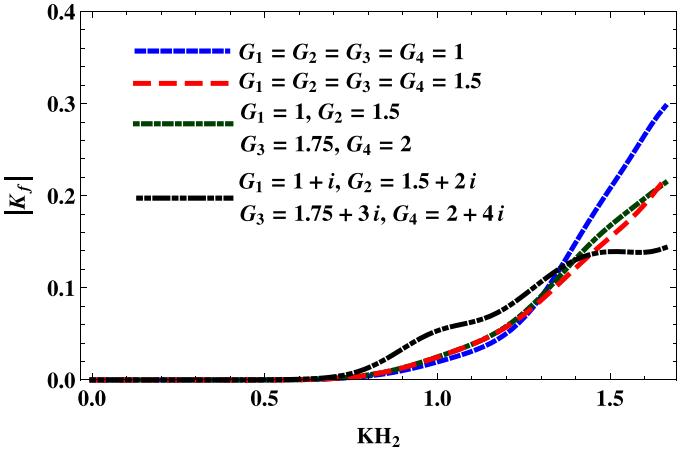

FIGURE 17. $|K_f|$ against KH_2 for $x_1 = 0.5, x_2 = 1.5, x_3 = 2.5, x_4 = 3.5, E = 0.4, M = 0.01, H_1 = H_3 = H_5 = H_7 = 0.05, H_4 = H_6 = H_8 = 1, \theta = 60°$.

forces varies with changes in both the wave number and the porous effect parameter. The observations from Figures 16 and 17 suggest that as the porosity increases, the coefficient of wave force decreases. Additionally, due to inertial effects, the values of $|K_f|$ for complex porosity are lower than those for real porosity. This implies that the presence of pores within the material affects the amplitude of wave forces differently depending on whether the porosity is real or complex. The decrease in wave force coefficient with increasing porosity likely reflects a reduction in the resistance offered by the porous material to the incoming waves. However, Figures 18 and 19 illustrate the effect of wave forces on flexible porous barriers across four different values of

https://doi.org/10.1017/S1446181124000257 Published online by Cambridge University Press

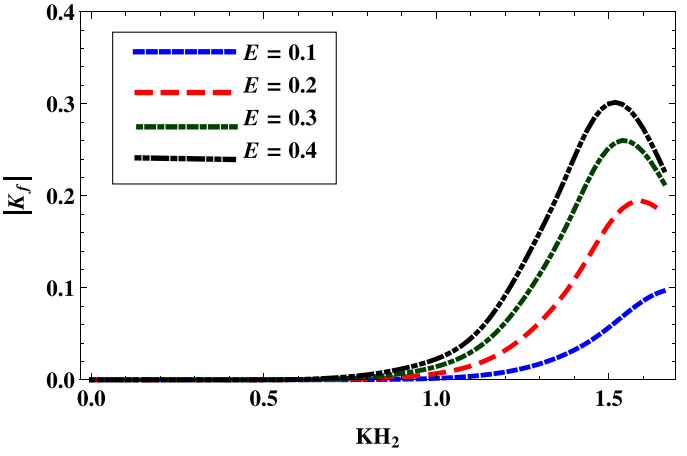

FIGURE 18. $|K_f|$ against KH_2 for $x_1 = 0.5, x_2 = 1.5, x_3 = 2.5, x_4 = 3.5, M = 0.01, G_1 = G_2 = G_3 = G_4 = 1$, $H_1 = H_3 = H_5 = H_7 = 0.05, H_4 = H_6 = H_8 = 1, \theta = 0°$.

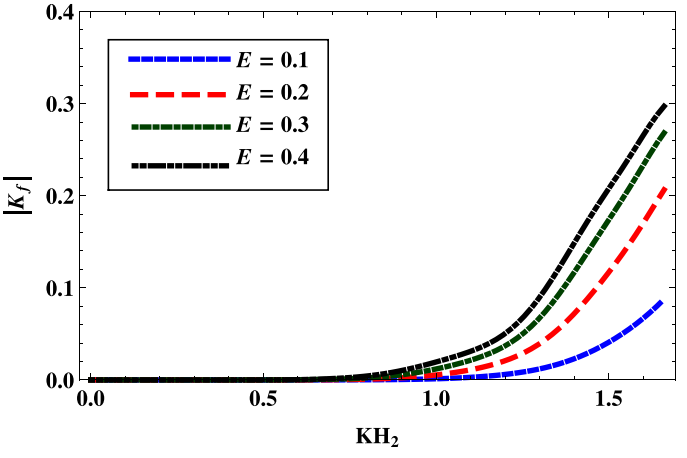

FIGURE 19. $|K_f|$ against KH_2 for $x_1 = 0.5, x_2 = 1.5, x_3 = 2.5, x_4 = 3.5, M = 0.01, G_1 = G_2 = G_3 = G_4 = 1$, $H_1 = H_3 = H_5 = H_7 = 0.05, H_4 = H_6 = H_8 = 1, \theta = 60°$.

flexural rigidity. It is observed from Figures 18 and 19 that the coefficient of wave force increases as the flexural rigidity of the porous plate increases. This suggests that flexural rigidity plays a significant role in enhancing the wave forces experienced by plates. A higher flexural rigidity likely results in increased resistance to bending or deformation when subjected to wave forces, leading to a higher coefficient of wave force. It is also observed that the maximum values of the wave forces $|K_f|$ are lower for obliquely incident waves compared with normal incident waves.

Figures 20 and 21 illustrate the amount of dissipated energy $|J|$ plotted against wave number KH_2 for various porosity values. These figures likely provide insights into

https://doi.org/10.1017/S1446181124000257 Published online by Cambridge University Press

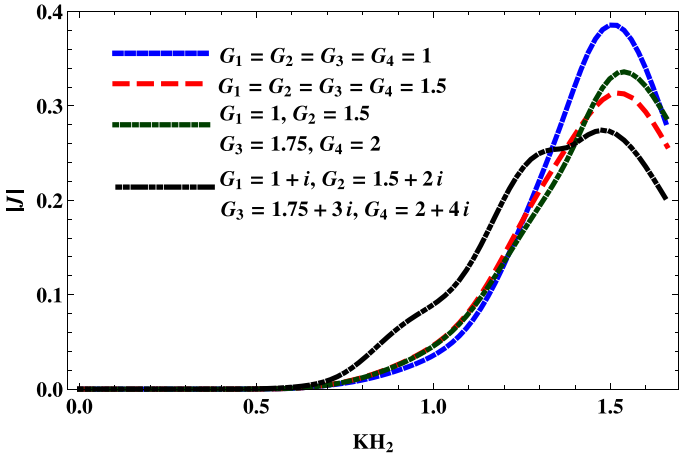

FIGURE 20. $|J|$ against KH_2 for $x_1 = 0.5, x_2 = 1.5, x_3 = 2.5, x_4 = 3.5, E = 0.4, M = 0.01, H_1 = H_3 = H_5 = H_7 = 0.05, H_4 = H_6 = H_8 = 1, \theta = 0°$.

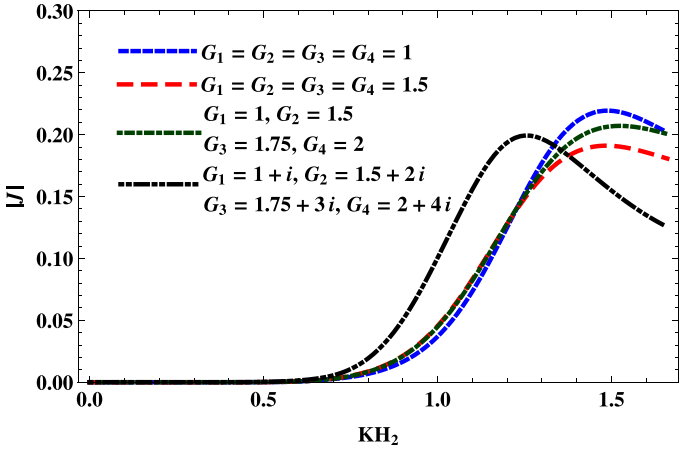

FIGURE 21. $|J|$ against KH_2 for $x_1 = 0.5, x_2 = 1.5, x_3 = 2.5, x_4 = 3.5, E = 0.4, M = 0.01, H_1 = H_3 = H_5 = H_7 = 0.05, H_4 = H_6 = H_8 = 1, \theta = 60°$.

how the dissipation of energy varies with changes in the wave number and porosity of the material. The observations from Figures 20 and 21 suggest that energy dissipation decreases as porosity increases. The addition of an imaginary part to the porous effect parameter results in a decrease in the value of dissipated energy. This suggests that incorporating certain imaginary components, possibly related to inertial effects, leads to a reduction in energy dissipation. However, dissipated energy $|J|$ for various flexural rigidity values is plotted against the wave number in Figures 22 and 23. Through Figures 22 and 23, it can be noticed that with increasing flexural rigidity of the barriers, the amount of dissipated energy $|J|$ increases. The higher flexural rigidity

https://doi.org/10.1017/S1446181124000257 Published online by Cambridge University Press

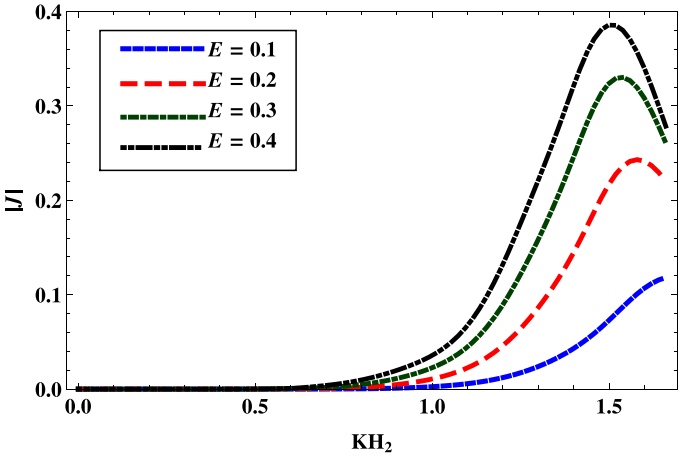

FIGURE 22. $|J|$ against KH_2 for $x_1 = 0.5, x_2 = 1.5, x_3 = 2.5, x_4 = 3.5, M = 0.01, G_1 = G_2 = G_3 = G_4 = 1$, $H_1 = H_3 = H_5 = H_7 = 0.05, H_4 = H_6 = H_8 = 1, \theta = 0°$.

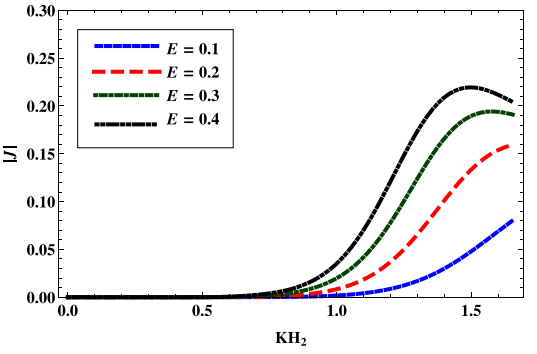

FIGURE 23. $|J|$ against KH_2 for $x_1 = 0.5, x_2 = 1.5, x_3 = 2.5, x_4 = 3.5, M = 0.01, G_1 = G_2 = G_3 = G_4 = 1$, $H_1 = H_3 = H_5 = H_7 = 0.05, H_4 = H_6 = H_8 = 1, \theta = 60°$.

likely allows the plates to absorb and dissipate more energy, resulting in higher values of $|J|$. Comparing Figures 20–23, it is observed that the maximum values of the dissipated energy $|J|$ are lower for obliquely incident waves compared with normal incident waves.

5. Conclusion

This paper presents a mathematical model and analysis of how surface waves interact with multiple flexible porous plates, using the Galerkin approximation method. This study computes and presents several hydrodynamics quantities, including reflection and transmission coefficients, hydrodynamic force, and energy dissipation. These hydrodynamics quantities are crucial for understanding how waves interact with the flexible porous plates and how they affect each other. The proposed model's

https://doi.org/10.1017/S1446181124000257 Published online by Cambridge University Press

validity is established by comparing its results with existing data from the literature. The computed reflection and transmission coefficients satisfy the energy identity for both permeable and impermeable flexible plates, affirming the model's accuracy. A decrease in the reflection coefficient with an increase in the angle of incidence is observed. Vertical plates are found to be better reflectors. Additionally, the oscillation of the reflection coefficient increases with increasing plate separation length, indicating interference effects within the flexible porous plates. The flexural rigidity of the plates significantly influences hydrodynamic coefficients. Higher flexural rigidity leads to increased reflection coefficients, especially in the presence of porosity. Wave load is initially higher at the first plate but decreases as waves propagate over subsequent plates, aligning with expectations. However, increasing porous effect parameters leads to a decrease in the reflection coefficient due to enhanced wave energy dissipation. Higher energy dissipation is achieved by minimizing the inertial effect of flexible porous plates, indicating their effectiveness in dissipating wave energy. Compared with rigid plates, multiple flexible porous plates demonstrate a reduction in reflection, dissipated energy and wave force. This finding suggests their suitability for constructing breakwaters and mitigating wave effects on coastal and marine facilities. Overall, the analysis provides valuable insights into the role of multiple flexible porous structures in dissipating wave energy and attenuating wave load, which is crucial for coastal and marine engineering applications.

Acknowledgements

The authors would like to gratefully acknowledge the Editor and Reviewers for their valuable comments and suggestions to improve the quality of the manuscript. This work is partially supported by a SERB, DST, India (grant number TAR/2022/000107).

References

[1] R. Ashok, C. Gunasundari and S. R. Manam, "Explicit solutions of the scattering problems involving vertical flexible porous structures", *J. Fluids Struct.* **99** (2020) Article ID: 103149; doi:10.1016/j.jfluidstructs.2020.103149.

[2] H. Behera and C. O. Ng, "Interaction between oblique waves and multiple bottom-standing flexible porous barriers near a rigid wall", *Meccanica* **53** (2018) 871–885; doi:10.1007/s11012–017–0789–8.

[3] S. Boral, T. Sahoo and M. H. Meylan, "Gravity wave interaction with an articulated submerged plate resting on a Winkler foundation", *Appl. Math. Model.* **113** (2022) 416–438; doi:10.1016/j.apm.2022.09.007.

[4] A. Chakrabarti, S. Banerjea, B. N. Mandal and T. Sahoo, "A Unified approach to problems of scattering of surface water waves by vertical barriers", *J. Aust. Math. Soc. Ser. B* **39** (1997) 93–103; doi:10.1017/S0334270000009231.

[5] R. Chakraborty and B. N. Mandal, "Scattering of water waves by a submerged thin vertical elastic plate", *Arch. Appl. Mech.* **84** (2014) 207–217; doi:10.1007/s00419-013-0794-x.

[6] R. Chakraborty, A. Mondal and R. Gayen, "Interaction of surface water waves with a vertical elastic plate: a hypersingular integral equation approach", *Z. Angew. Math. Phys.* **67** (2016) 115; doi:10.1007/s00033-016-0709-0.

[7] A. T. Chwang, "A porous wave maker theory", *J. Fluid Mech.* **132** (1983) 395–406; doi:10.1017/S0022112083001676.

[8] S. De, B. N. Mandal and A. Chakrabarti, "Use of Abel integral equations in water wave scattering by two surface piercing barriers", *Wave Motion* **47** (2010) 279–288; doi:10.1016/j.wavemoti.2009.12.002.
[9] W. R. Dean, "On the reflection of surface waves by submerged plane barriers", *Math. Proc. Cambridge Philos. Soc.* **41** (1945) 231–238; doi:10.1017/S030500410002260X.
[10] D. V. Evans and C. A. N. Morris, "Complementary approximations to the solution of a problem in water waves", *J. Inst. Math. Appl.* **10** (1972) 1–9; doi:10.1093/imamat/10.1.1.
[11] R. Gayen and A. Mondal, "Scattering of water waves by a pair of vertical porous plates", *Geophys. Astrophys. Fluid Dyn.* **109** (2015) 480–496; doi:10.1080/03091929.2015.1076812.
[12] M. U. Hassan, M. H. Meylan and M. A. Peter, "Water-wave scattering by submerged elastic plates", *QJMAM* **62** (2009) 321–344; doi:10.1093/qjmam/hbp008.
[13] S. R. Heller and H. N. Abramson, "Hydroelasticity: a new naval science", *J. Amer. Soc. Naval Eng.* **71**(2) (1959) 205–209; doi:10.1111/j.1559-3584.1959.tb02326.x.
[14] M. Isaacson, J. Baldwin, S. Premasiri and G. Yang, "Wave interactions with double slotted barriers", *Appl. Ocean Res.* **21** (1999) 81–91; doi:10.1016/S0141-1187(98)00039-X.
[15] M. Isaacson, S. Premasiri and G. Yang, "Wave interactions with vertical slotted barriers", *J. Waterway Port Coastal Ocean Eng.* **124** (1998) 118–126; doi:10.1061/(ASCE)0733-950X(1998)124:3(118).
[16] R. J. Jarvis, "The scattering of surface waves by two vertical plane barriers", *J. Inst. Math. Appl.* **7** (1971) 207–215.
[17] D. Karmakar and C. G. Soares, "Wave transformation due to multiple bottom-standing porous barriers", *Ocean Eng.* **80** (2014) 50–63; doi:10.1016/j.oceaneng.2014.01.012.
[18] N. S. Karp and C. F. Karal, "The elastic field behaviour in the neighbourhood of a crack of arbitrary angle", *Comm. Pure Appl. Math.* **15** (1962) 413–421; doi:10.1002/cpa.3160150404.
[19] H. Levine and E. Rodemich, "*Scattering of surface waves on an ideal fluid*", Technical Report 78, Mathematics and Statistics Laboratory, Standford University, 1958.
[20] A. J. Li, Y. Liu and H. J. Li, "Accurate solutions to water wave scattering by vertical thin porous barriers", *Math. Problem Eng.* **2015** (2015) 1–11; doi:10.1155/2015/985731.
[21] Y. Liu, A. J. Li and Z. B. Fang, "Oblique wave scattering by porous breakwaters/seawalls: novel analytical solutions based on contour integral without finding complex roots", *Appl. Ocean Res.* **101** (2020) Article ID: 102258; doi:10.1016/j.apor.2020.102258.
[22] I. J. Losada, M. A. Losada and A. J. Roldan, "Propagation of oblique incident waves past rigid vertical thin barriers", *Appl. Ocean Res.* **14** (1992) 191–199; doi: 10.1016/0141-1187(92)90014-B
[23] C. Macaskill, "Reflection of water waves by a permeable barrier", *J. Fluid Mech.* **75** (1979) 141–157; doi:10.1017/S0022112079001385.
[24] S. R. Manam and M. Sivanesan, "Scattering of water waves by vertical porous barriers: an analytical approach", *Wave Motion* **67** (2016) 89–101; doi:10.1016/j.wavemoti.2016.07.008.
[25] B. N. Mandal and A. Chakrabarti, *Water wave scattering by barriers*, 1st edn (WIT Press, Southampton, UK, 2000).
[26] P. McIver, "Scattering of surface waves by two surface piercing vertical barriers", *IMA J. Appl. Math.* **35**(1) (1985) 1–17; doi:10.1093/imamat/35.339.
[27] M. Meylan, "A flexible vertical sheet in waves", *Int. J. Offshore Polar Eng.* **5** (1995) 105–110.
[28] C. A. N. Morris, "A variational approach to an unsymmetric water wave scattering problem", *J. Eng. Math.* **9** (1975) 291–300; doi:10.1007/BF01540666.
[29] J. N. Newman, "Interaction of water waves with two closely spaced vertical obstacles", *J. Fluid Mech.* **66** (1974) 97–106; doi:10.1017/S0022112074000085.
[30] M. A. Peter and M. Meylan, "A general spectral approach to the time-domain evolution of linear water waves impacting on a vertical elastic plate", *SIAM J. Appl. Math.* **70** (2010) 2308–2328; doi:10.1137/09075655.
[31] D. Porter, "The transmission of surface waves through a gap in a vertical barrier", *Math. Proc. Cambridge Philos. Soc.* **71** (1972) 411–421; doi:10.1017/S0305004100050647.
[32] R. Porter and D. V. Evans, "Complementary approximations to solve wave scattering by vertical barriers", *J. Fluid Mech.* **294** (1995) 155–180; doi:10.1017/S0022112095002849.

[33] R. Roy, S. De and B. N. Mandal, "Water wave scattering by three thin vertical barriers arranged asymmetrically in deep water", *Fluid Dyn. Res.* **51** (2019) Article ID 045508, 23 pages; doi:10.1088/1873-7005/ab2d4d.

[34] A. Sasmal and S. De, "Oblique water wave diffraction by two vertical porous barriers with nonidentical submerged gaps", *Meccanica* **54** (2019) 1525–1544; doi:10.1007/s11012-019-01031-1.

[35] A. Sasmal and S. De, "Energy dissipation and oblique wave diffraction by three asymmetrically arranged porous barriers", *Ships Offshore Struct.* **17** (2020) 105–115; doi:10.1080/17445302.2020.1816783.

[36] A. Sasmal and S. De, "Hydroelastic analysis of surface gravity wave interaction with multiple flexible porous structures", *J. Fluids Struct.* **120** (2023) Article ID: 103906; doi:10.1016/j.jfluidstructs.2023.103906.

[37] A. Sasmal and S. De, "Mitigation of wave force and dissipation of energy by multiple arbitrary porous barriers", *Waves Random Complex Media* **34** (2024) 523–546; doi:10.1080/17455030.2021.1915514.

[38] A. Sasmal, S. Paul and S. De, "Effect of porosity on oblique wave diffraction by two unequal vertical porous barriers", *J. Mar. Sci. Appl.* **18** (2019) 417–432; doi:10.1007/s11804-019-00107-4.

[39] M. Singh and R. Gayen, "Scattering of linear gravity-capillary waves by a completely submerged vertical porous elastic plate", *Waves Random Complex Media* (2022) 1–21; doi: 10.1080/17455030.2022.2120220.

[40] S. Singh and R. Kaligatla, "The combined refraction-diffraction effect on water wave scattering by a vertical flexible-porous structure", *J. Fluids Struct.* **116** (2023) Article ID: 103791; doi:10.1016/j.jfluidstructs.2022.103791.

[41] C. M. Smith, "Some problems in linear water wave theory", Ph. D. Thesis, University of Bristol, Bristol, 1983.

[42] M. J. A. Smith, M. A. Peter, I. D. Abrahams and M. H. Meylan, "On the Wiener–Hopf solution of water-wave interaction with a submerged elastic or poroelastic plate", *Proc. Roy. Soc. London A Math. Phy. Sci.* **476** (2020) Article ID: 2242; doi:10.1098/rspa.2020.0360.

[43] C. K. Sollitt and R. H. Cross, "Wave transmission through permeable breakwaters", *Coastal Eng. Proc.* **1** (1972) 1827–1846; doi:10.1061/9780872620490.106.

[44] I. V. Sturova, "The effect of periodic surface pressure on a rectangular elastic plate floating on shallow water", *ZAMM* **70** (2006) 378–386; doi:10.1016/j.jappmathmech.2006.07.016.

[45] F. Ursell, "The effect of a fixed vertical barrier on surface waves in deep water" *Math. Proc. Cambridge Philos. Soc.* **43** (1947) 374–382; doi:10.1017/S0305004100023604.

[46] W. E. Williams "Note on the scattering of water waves by a vertical barrier", *Math. Proc. Cambridge Philos. Soc.* **62** (1988) 507–509; doi:10.1017/S0305004100040135.

[47] Y. S. Wu, "Numerical and experimental hydroelasticity of marine structures–a review", in: *ICHD'94 Proc. Int. Conf. on Hydrodynamics*, Wuxi, China, 30 October–3 November 1994 (editorial board for Journal of Hydrodynamics), 30–41.

[48] X. Yu, "Diffraction of water waves by porous breakwaters", *J. Waterway Port Coastal Ocean Eng.* **121** (1995) 275–282; doi:10.1061/(ASCE)0733-950X(1995)121:6(275).

[49] X. Yu and A. T. Chwang, "Wave motion through porous structures", *ASCE J. Eng. Mech.* **120**(5) (1994) 989–1008; doi:10.1061/(ASCE)0733-9399(1994)120:5(989).

[50] S. Zheng, M. H. Meylan, L. Fan, D. Greaves and G. Iglesias, "Wave scattering by a floating porous elastic plate of arbitrary shape: a semi-analytical study", *J. Fluids Struct.* **92** (2020) Article ID: 102827; doi:10.1016/j.jfluidstructs.2019.102827.

[51] S. Zheng, M. H. Meylan, D. Greaves and G. Iglesias, "Water-wave interaction with submerged porous elastic disks", *Phys. Fluids.* **32** (2020) Article ID: 047106; doi:10.1063/5.0006119.

[52] S. Zheng, M. H. Meylan, G. Zhu, D. Greaves and G. Iglesias, "Hydroelastic interaction between water waves and an array of circular floating porous elastic plates", *J. Fluid Mech.* **900** (2020) Article ID: A20; doi:10.1017/jfm.2020.508.